Optimized Biorthogonal Shape Adaptive Wavelets

Alfred Mertins
The University of Western Australia
Dept. of Electrical and Electronic Engineering
Nedlands 6907 WA, AUSTRALIA, mertins@ee.uwa.edu.au

Abstract

This paper presents shape adaptive wavelet transforms for object-based image coding. Methods for recovering moment properties that are valid for the original filters and wavelets, but that get lost in the boundary regions of shape adaptive transforms, are presented. Furthermore, methods for equalizing the energies of the boundary wavelets are shown. This equalization allows to avoid that white quantization noise (introduced in the subbands) appears as highly colored noise in the reconstructed image.

1 Introduction

The principle of the discrete wavelet transform (DWT) is to represent a given signal $x(t)$ via a linear series expansion where all basis functions are derived from a single wavelet $\psi(t)$ by dilation and translation [1]. The coefficients of the expansion are computed by taking inner products of $x(t)$ with translated and dilated versions of a dual wavelet $\tilde{\psi}(t)$. However, instead of seeking suitable functions $\psi(t)$ and $\tilde{\psi}(t)$ and implementing them directly, we may use cascades of perfect reconstruction (PR) two-channel filter banks for constructing the wavelets and implementing the transform [1, 2, 3]. Fig. 1 shows such a filter bank. Under the condition of regularity, two so-called scaling functions, $\phi(t)$ and $\tilde{\phi}(t)$, and the wavelets $\psi(t)$ and $\tilde{\psi}(t)$ can be derived from the discrete filters [1, 3]. The PR condition for the discrete case then also ensures PR for the DWT, so that any finite-energy signal $x(t)$ can be represented without error. Moreover, due to critical subsampling, the number of wavelet coefficients is equal to the number of input samples for the discrete-time filter bank.

It is important to notice that the above considerations only hold for infinitely sized signals. For signals of finite size, special processing steps have to be applied in the boundary regions in order to result in a support preservative transform [4, 5, 6, 7, 8, 9]. More recently, the boundary processing methods have been applied in order to achieve shape adaptive discrete wavelet transforms

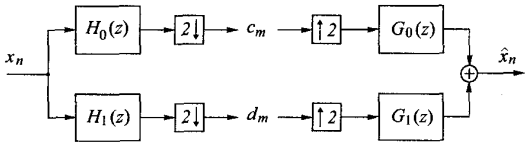

Fig. 1. Two-channel filter bank.

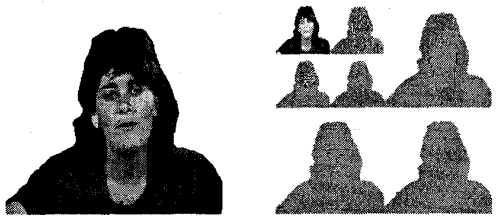

Fig. 2. Shape adaptive wavelet transform. (a) original; (b) transformed image.

(SA DWTs) for decomposing arbitrary regions of images [10, 11, 12]. Fig. 2 shows an example of such a support preservative SA DWT.

In this paper, optimized SA DWTs for image coding purposes are proposed. Since images mainly contain low-frequency content and typically have a large DC component, it is important for compression, that the DC value of an input signal only affects the lowpass band. Moreover, it is desirable that polynomial signals of first and higher order can be represented via the lowpass component only. In the interior region of an object, where the wavelet basis is not affected by the region boundary, this is guaranteed by the approximation properties of the wavelet in use. For example, if the wavelet $\psi(t)$ has N_ψ vanishing moments, then $\int_{-\infty}^{\infty} t^n \psi(t) dt = 0$ for $n = 0, \ldots, N_\psi - 1$. Thus, polynomial input signals up to order $N_\psi - 1$ are represented by the lowpass band only. Similar moment properties hold for the discrete filters, which are used to carry out the DWT [13]. For example, the analysis highpass $h_1(n)$ satisfies $\sum_n n^k \; h_1(n) = 0$ for $k = 0, \ldots, N_\psi - 1$.

In the boundary regions, the moment properties men-

0-8186-8821-1/98 $10.00

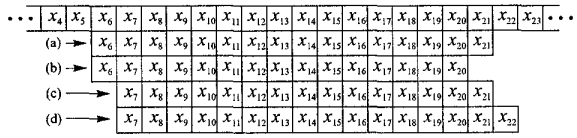

Fig. 3. Different cases in a shape adaptive scheme.

tioned above are not necessarily preserved. This problem has e.g. been raised in [11], where boundary filters were designed in such a way that several moment conditions are satisfied by the analysis filters, resulting in wavelets that allow time-scale image analysis with low boundary distortion. For compression purposes, however, the properties of the synthesis functions are as important as those of the analysis ones. Thus, both sides should be considered jointly when designing boundary filters. In the following sections, we study possibilities of recovering moment properties in the boundary regions of arbitrarily shaped images. Furthermore, we study methods for equalizing the energies of the boundary wavelets. This is important in order to equalize the propagation of quantization errors from the subbands to the output. The wavelets under consideration are biorthogonal linear-phase wavelets generated from odd and even-length filters, respectively.

2 Arbitrary-Length Signals

The 2-D SA-DWT is mainly based on schemes for the decomposition of arbitrary-length 1-D signals. Since signal segments may start and stop at even and odd positions the following four cases need to be considered:

(i) even start and odd stop position
(ii) even start and even stop position
(iii) odd start and odd stop position
(iv) odd start and even stop position

Fig. 3 shows an example. It is easily seen that the decomposition in one direction has to take care of the start and stop position of a segment, so that the subsequent decomposition in the second direction can maximally exploit the correlation between pixels. In the example, it is assumed that all rows essentially contain the same values. Thus, each vertical decomposition should lead to equal lowpass and zero highpass coefficients. This should even be the case if the horizontal decomposition is carried out prior the vertical one.

As the initial method for a support-preservative decomposition (prior optimization), we consider symmetric extension. Both odd and even-length linear-phase filters will be addressed.

2.1 Odd-Length Filters

The principle is depicted in Fig. 4(a) for a length-8 signal $x_0, x_1, \ldots, x_7$ and symmetric filters with impulse responses $\{A, B, C, B, A\}$ for the lowpass and $\{-a, b, -a\}$ for the highpass. The upper row shows the extended input signals, where the given input samples are shown in solid boxes. The lowpass and highpass subband samples, c_n and d_n respectively, are computed by taking the inner products of the impulse responses in the displayed positions with the corresponding part of the extended input signal. Note that only four different lowpass and highpass coefficients, named as $c_0, \ldots, c_3$ and $d_0, \ldots, d_3$, occur. Only these eight different coefficients need to be stored or transmitted. At the receiver side, the subband signals can be extended accordingly, and the complete analysis/synthesis scheme is support preservative and it provides PR.

An interesting property of odd-length biorthogonal linear-phase filters is the fact that symmetric reflection can be applied at every start position of a segment (even or odd) and for any segment length. In order to illustrate this, Fig. 4(b) again shows the decomposition of a length-8 signal, now starting at an odd position. As in Fig. 4(a) we get four lowpass and four highpass coefficients. The processing of odd-length segments starting at even or odd positions is carried out by combining the schemes in Figs. 4(a) and (b).

2.2 Even-Length Filters

Symmetric reflection for even-length filters is depicted in Figs. 4(c) and (d). As before, decomposition schemes for odd-length segments are derived by combining the shown reflection methods.

Although both schemes in Figs. 4(c) and (d) are support preservative, the one in Fig. 4(d) normally results in more lowpass than highpass coefficients. This can be avoided by introducing an additional highpass coefficient $d_0 = c_1 - c_0$ and neglecting c_0.

3 Vanishing Moments at the Boundaries

The symmetric extension method described in the previous section already has the property that the analysis wavelets will have at least one vanishing moment, even in the boundary regions.[1] This is obvious, because for a DC input signal $x_n = 1$, $n = 0, \ldots, N-1$, the extended signal becomes $x_n^E = 1$, $n \in \mathbb{Z}$, which means that the zero of the analysis highpass at $z = 1$ is preserved in the boundary regions. Since the extensions in Figs. 4(a) and (b) for odd-length filters are carried out without repeating the first or last sample, a signal $x_n = (-1)^n$, $n = 0, \ldots, N-1$, is extended as $x_n^E = (-1)^n$, $n \in \mathbb{Z}$. This means that in this case also the zero of the analysis lowpass at $z = -1$ is preserved in the boundary regions.

Let us consider one of the cases (i)–(iv) described in Section 2 and let us write the two-channel decomposition

[1] It is assumed that $H_1(1) = G_1(1) = 0$, which is a minimum requirement for regularity.

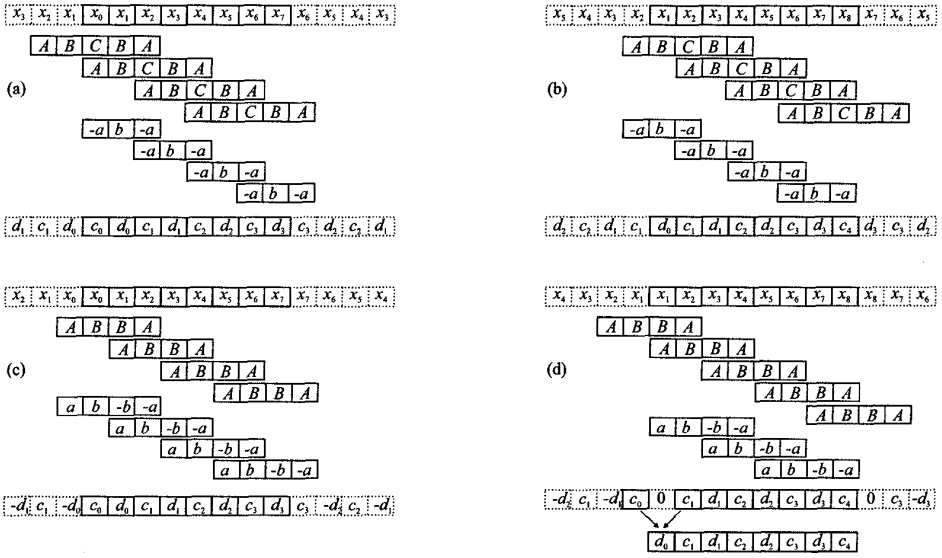

Fig. 4. Symmetric reflection for even-length signals. (a) odd-length filters, segment starting at an even position; (b) odd-length filters, segment starting at an odd position. (c) even-length filters, segment starting at an even position; (d) even-length filters, segment starting at an odd position.

as

$$\boldsymbol{y} = \boldsymbol{H}\,\boldsymbol{x} \tag{1}$$

The rows of the matrix $\boldsymbol{H}$ contain the time-shifted analysis impulse responses in reversed order, while the vectors $\boldsymbol{x}$ and $\boldsymbol{y}$ contain the input and the subband samples in increasing order (e.g. $\boldsymbol{y}^T = [c_0, d_0, c_1, d_1, \ldots]$). In the upper left and the lower right corner of $\boldsymbol{H}$, we find the boundary filters, which are generated by folding back the original impulse responses according to the symmetric reflection methods described in the previous section.

In order to optimize the boundary filters, let us partition $\boldsymbol{y}$ and $\boldsymbol{H}$ such that

$$\boldsymbol{y} = \left[\boldsymbol{y}_1^T, \boldsymbol{y}_2^T, \boldsymbol{y}_3^T\right]^T, \qquad \boldsymbol{y}_k = \boldsymbol{H}_k\,\boldsymbol{x}, \tag{2}$$

where $\boldsymbol{y}_1$ and $\boldsymbol{y}_3$ contain the subband samples produced by the boundary filters. The boundary filter manipulation may be written in the following form, where the vectors $\boldsymbol{v}_k$ contain the new subband samples:

$$\boldsymbol{v}_k = \boldsymbol{U}_k \boldsymbol{H}_k\,\boldsymbol{x}, \qquad \boldsymbol{U}_2 = \boldsymbol{I}. \tag{3}$$

This means, apart from the boundaries the signal is processed as usual (indicated by the identity matrix). In the boundary regions, the impulse responses of the boundary filters are linearly combined ($\boldsymbol{U}_1$ and $\boldsymbol{U}_3$) in order to result in better boundary filters. Note that the inverse operation is required on the synthesis side.

If certain moment properties should be met by the optimized filters, the matrices $\boldsymbol{U}_1$ and $\boldsymbol{U}_3$ have to be restricted in a certain way. For this, let us formulate the requirements as

$$\boldsymbol{V}_k = \boldsymbol{U}_k\,\boldsymbol{Y}_k \tag{4}$$

where $\boldsymbol{Y}_k = \boldsymbol{H}_k\,[\boldsymbol{t}^{(1)}, \boldsymbol{t}^{(2)}, \ldots, \boldsymbol{t}^{(I)}]$ contains the actual responses to specific input signals $\boldsymbol{t}^{(i)}$, $i = 1, 2, \ldots, I$ and $\boldsymbol{V}_k = [\boldsymbol{v}_k^{(1)}, \boldsymbol{v}_k^{(2)}, \ldots, \boldsymbol{v}_k^{(I)}]$ contains the desired responses to these signals. For example, if we simply want to preserve the zeros of the boundary highpass and lowpass filters at $\omega = 0$ and $\omega = \pi$, which are already present due to the reflection method, we choose $\boldsymbol{V}_k = \boldsymbol{Y}_k = \boldsymbol{H}_k\,[\boldsymbol{t}^{(1)}, \boldsymbol{t}^{(2)}]$ where $\boldsymbol{t}^{(1)} = [1, 1, 1, 1, \ldots]^T$ and $\boldsymbol{t}^{(2)} = [1, -1, 1, -1, \ldots]^T$. If we want to add conditions on the response to linear polynomial signals, the vector $\boldsymbol{t}^{(3)} = [1, 2, 3, 4, \ldots]^T$ has to be included and the desired response $\boldsymbol{v}_k^{(3)}$ has to be specified.

The matrix $\boldsymbol{U}_k$ can be parameterized as follows:

$$\boldsymbol{U}_k = \boldsymbol{Y}_k^{+} + \boldsymbol{P}_k \boldsymbol{Z}_k^T \tag{5}$$

where $\boldsymbol{Z}_k$ contains the basis of the nullspace of $\boldsymbol{Y}_k$ such that $\boldsymbol{Z}_k^T \boldsymbol{Y}_k = \boldsymbol{0}$. The matrix $\boldsymbol{Y}_k^{+}$ is the pseudo inverse of $\boldsymbol{Y}$, and $\boldsymbol{P}$ contains the free design parameters, which can be chosen in order to optimize $\boldsymbol{U}_k$. As long as the number of conditions I is small enough to ensure that $\boldsymbol{Y}_k^{+} \boldsymbol{Y}_k = \boldsymbol{I}$, the requirements (4) are fulfilled exactly. If more conditions are added, such that $\boldsymbol{Y}_k^{+} \boldsymbol{Y}_k \neq \boldsymbol{I}$, (4) is satisfied in the least squares sense, but there are no further free design parameters for optimization.

For extremely short segments, the boundary filters for the left and right boundary merge and $\boldsymbol{H}_2$ vanishes. In these cases, we replace the matrices $\boldsymbol{U}_1$ and $\boldsymbol{U}_3$ by a common matrix $\boldsymbol{U}$, such that $\boldsymbol{v} = \boldsymbol{U}\boldsymbol{H}\boldsymbol{x}$, where $\boldsymbol{U} = \boldsymbol{Y}^+ + \boldsymbol{P}\boldsymbol{Z}^T$. Then, for each segment length and starting position (even or odd), a different matrix $\boldsymbol{U}\boldsymbol{H}$ will be implemented. The optimization of the matrices $\boldsymbol{U}$ is carried out in the same way as the optimization of $\boldsymbol{U}_k$.

4 Filter Optimization

Folding back the impulse responses according to the symmetric reflection method results in new filters with different energies. This is easily seen by considering the left boundary in Fig. 4(a). The first boundary lowpass has the impulse response $\{2A, 2B, C\}$ while the normal impulse response is $\{A, B, C, B, A\}$. The energies differ by $2A^2 + 2B^2$. Since the complete 2-D wavelet decomposition of an arbitrary region is carried out by cascading several 1-D support preservative decompositions, this effect can accumulate and result in iterated filters and associated wavelets with energies that may differ significantly from their nominal value. Both, the analysis and the synthesis bank are affected.

Large differences in the filter's energies (belonging to the same subband) are especially critical for the synthesis side, because quantization errors introduced in the subbands will propagate to the output with amplifications being equal to the associated synthesis filters' energies. Thus, white quantization noise introduced in the subbands may occur at the output as extremely colored noise when some of the boundary synthesis filters have very high energies.

Since we are interested in equalizing the energies of the boundary filters and keeping these energies close to one, we look for matrices $\boldsymbol{U}_k$ that minimize an expression of the form

$$\begin{aligned} &\lambda_1 \left\| \mathrm{diag}\left\{ \boldsymbol{U}_k \boldsymbol{H}_k \boldsymbol{H}_k^T \boldsymbol{U}_k^T \right\} - \mathbf{1}_k \right\|^2 \\ &+\lambda_2 \left\| \mathrm{diag}\left\{ (\boldsymbol{U}_k^{-1})^T \boldsymbol{G}_k^T \boldsymbol{G}_k \boldsymbol{U}_k^{-1} \right\} - \mathbf{1}_k \right\|^2 \end{aligned} \tag{6}$$

Herein, $\mathbf{1}_k$ is a vector of appropriate size containing ones, and $\mathrm{diag}\{\cdot\}$ means a vector containing the diagonal elements of a matrix. The matrices $\boldsymbol{G}_k$ are the corresponding partitions of the synthesis matrix $\boldsymbol{G} = \boldsymbol{H}^{-1}$. The pre-factors λ_1 and λ_2 are introduced in order to allow weighting of the two criteria included in (6).

Although minimizing the above expression leads to optimal filters for the 1-D case, it does not reflect all requirements in a 2-D shape adaptive scheme. Here, different rows/columns can start and stop at arbitrary positions, and filtering in one direction should cause minimal distortion in the second one. Thus, when optimizing boundary filters we have to take care of the compaction properties in both directions. According to the method in [9] for the orthonormal case, this can be done as follows:

Let $\boldsymbol{x}_\infty$ to be an infinite-length 1-D stochastic process and let $\boldsymbol{x} = \boldsymbol{C}_x \boldsymbol{x}_\infty$ be a finite-length segment of $\boldsymbol{x}_\infty$. For example, $\boldsymbol{x}_\infty$ may be the first and $\boldsymbol{x}$ may be one of the other rows in Fig. 3. Also, let $\boldsymbol{w}_\infty = \boldsymbol{F}\boldsymbol{x}_\infty$ be the vector of subband samples computed from $\boldsymbol{x}_\infty$, and let $\boldsymbol{w} = \boldsymbol{C}_w \boldsymbol{w}_\infty$ be that partition of $\boldsymbol{w}_\infty$ that corresponds to $\boldsymbol{v} = \boldsymbol{U}\boldsymbol{H}\boldsymbol{x}$. Like $\boldsymbol{y}$ and $\boldsymbol{v}$, also $\boldsymbol{w}$ may be further partitioned into $\boldsymbol{w}_1$, $\boldsymbol{w}_2$, and $\boldsymbol{w}_3$. Requiring $E\{\|\boldsymbol{v}_k - \boldsymbol{w}_k\|^2\} \stackrel{!}{=} \min$ then yields well-aligned boundary filters. Thus, the following objective function is proposed

$$\begin{aligned} C_k(\boldsymbol{P}_k) \;=\; & \lambda_1 \left\| \mathrm{diag}\left\{ \boldsymbol{U}_k \boldsymbol{H}_k \boldsymbol{H}_k^T \boldsymbol{U}_k^T \right\} - \mathbf{1}_k \right\|^2 \\ & + \lambda_2 \left\| \mathrm{diag}\left\{ (\boldsymbol{U}_k^{-1})^T \boldsymbol{G}_k^T \boldsymbol{G}_k \boldsymbol{U}_k^{-1} \right\} - \mathbf{1}_k \right\|^2 \\ & + \lambda_3 \, E\{\|\boldsymbol{v}_k - \boldsymbol{w}_k\|^2\} \end{aligned} \tag{7}$$

In the experiments discussed below, $\lambda_1 = 0.75$, $\lambda_2 = 1$, $\lambda_3 = 2$ have been used. The process $\boldsymbol{x}_\infty$, that generates the random vectors $\boldsymbol{v}_k$ and $\boldsymbol{w}_k$ in (7), was defined as an AR(1) process with correlation coefficient 0.95.

For the optimized filters, the noise amplification factor for a four-band decomposition typically varies between 0.98 and 1.02, which means, it can be considered as being independent of the location. Exceptions occur for segments of length one, two, and three, where we do not have sufficient design freedom in order to fully equalize the noise amplification. Moreover, if more decomposition levels are used, the factors may slightly vary from their nominal value, because in the biorthogonal case, the energy of an upsampled and interpolated filter is not necessarily equal to the energy of the filter itself, even if the filter is normalized. That is, if $\sum_n g_0^2(n) = 1$ then $\sum_n f^2(n) \neq 1$ in general, where $f(2n) = \sum_m g_0(n-m) g_0(2m)$, $f(2n+1) = \sum_m g_0(n-m) g_0(2m+1)$.

5 Coding Results

Coding results are presented for the camera man image using the segmentation depicted in Fig. 5. Fig. 6 shows a comparison of rate-distortion curves for optimized and non-optimized boundary filters. During optimization, only the 0^{th} moments of the boundary filters were considered, because coding experiments have shown that forcing more moments to vanish results in loss of compression performance. For the even-length filters, the modification described in Section 2.2 for turning the first lowpass into a highpass coefficient was used. This allows simple in-place computation of the 2-D SA DWT.

The rate-distortion curves show that odd-length filters in combination with the reflection scheme from Figs. 4(a)

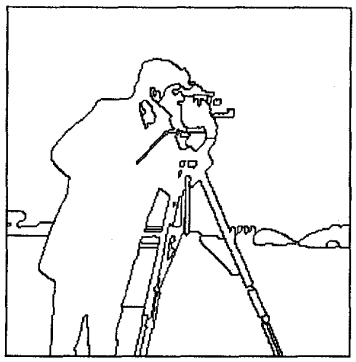

Fig. 5. Segmentation of the camera man image.

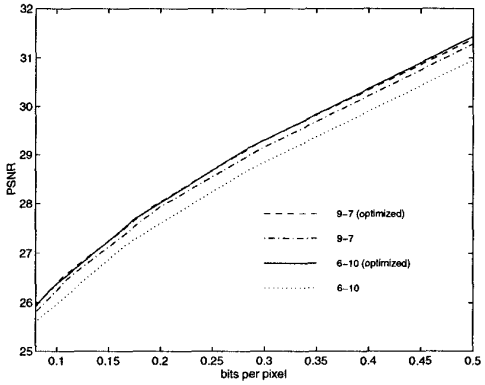

Fig. 6. Rate-distortion results for the camera man image. (9-7 filters from [14]; 6-10 filters from [15])

and (b) already yield near-optimum results. Even-length filters with non-optimized boundary processing perform relatively poor. However, with boundary optimization they yield excellent results.

6 Conclusions

In this paper, methods for designing optimal boundary filters for SA wavelet transforms have been presented. The results show that optimization yields significant improvement of the performance, especially for even-length filters, where direct reflection methods perform relatively poor.

References

[1] I. Daubechies, "Orthonormal bases of compactly supported wavelets," *Comm. Pure and Appl. Math.*, vol. XLI, pp. 909–996, 1988.

[2] A. Cohen, I. Daubechies, and J. C. Feauveau, "Biorthogonal bases of compactly supported wavelets," *Comm. Pure and Appl. Math.*, vol. XLV, pp. 485–560, 1992.

[3] M. Vetterli and C. Herley, "Wavelets and filter banks: Theory and design," *IEEE Trans. Acoust., Speech, Signal Processing*, vol. 40, pp. 2207–2232, September 1992.

[4] J. Woods and S. O'Neil, "Subband coding of images," *IEEE Trans. Acoust., Speech, Signal Processing*, vol. 34, pp. 1278–1288, May 1986.

[5] M.J.T. Smith and S.L. Eddins, "Analysis/synthesis techniques for subband coding," *IEEE Trans. Acoust., Speech, Signal Processing*, pp. 1446–1456, Aug. 1990.

[6] H. J. Barnard, J. H. Weber, and J. Biemond, "Efficient signal extension for subband/wavelet decomposition of arbitrary length signals," in *Proc. SPIE, VCIP*, vol. 2094, pp. 966–975, November 1993.

[7] L. Chen, T. Nguyen, and K. P. Chan, "Symmetric Extension Methods for M-Channel PR LP FIR Analysis/Synthesis Systems," in *Proc. IEEE Int. Symp. Circuits and Systems*, London, UK, pp. 2.273 – 2.276, June 1994.

[8] C. Herley, "Boundary filters for finite-length signals and time-varying filter banks," *IEEE Trans. Circuits and Systems II*, vol. 42, pp. 102–114, February 1995.

[9] A. Mertins, "Time-varying and support preservative filter banks: Design of optimal transition and boundary filters via SVD," in *Proc. IEEE Int. Conf. Acoust., Speech, Signal Processing*, Detroit, USA, pp. 1316–1319, May 1995.

[10] H. J. Barnard, J. H. Weber, and J. Biemond, "A region-based discrete wavelet transform," in *Proc. European Signal Processing Conference*, pp. 1234–1237, September 1994.

[11] M. Coffrey, "Boundary compensated wavelet bases," in *Proc. IEEE Int. Conf. Acoust., Speech, Signal Processing*, München, Germany, pp. 2129–2132, May 1997.

[12] J. Apostolopoulos and J. Lim, "Transform/subband representation for signals with arbitrarily shaped regions of support," in *Proc. IEEE Int. Conf. Acoust., Speech, Signal Processing*, München, Germany, pp. 2097–2100, May 1997.

[13] S. Mallat, "A theory for multiresolution signal decomposition: The wavelet representation," *IEEE Trans. on Patt. Anal. and Mach. Intell.*, vol. 2, pp. 674–693, July 1989.

[14] M. Antonini, M. Barlaud, P. Mathieu, and I. Daubechies, "Image coding using wavelet transform," *IEEE Trans. Image Processing*, vol. 1, pp. 205–220, April 1992.

[15] J. D. Villasenor, B. Belzer, and J. Liao, "Wavelet filter evaluation for image compression," *IEEE Trans. Image Processing*, vol. 4, pp. 1053–1060, August 1995.